Journal of Nuclear Materials 396 (2010) 119–129

Contents lists available at ScienceDirect

Journal of Nuclear Materials

journal homepage: www.elsevier.com/locate/jnucmat

Stress state dependence of in-reactor creep and swelling. Part 2: Experimental results

M.M. Hall Jr. [a,*], J.E. Flinn [b]

[a] Bettis Laboratory, 1366 Hillsdale Drive, Monroeville, PA, USA
[b] Argonne National Laboratory, 164 Fair Hills Circle, Idaho Falls, ID, USA

ARTICLE INFO

Keywords:
Fast reactor materials
Steels, Austenitic
Swelling: metals and alloys
Creep and stress relaxation
Experimental techniques
Theory and modeling

ABSTRACT

Irradiation creep constitutive equations, which were developed in Part I, are used here to analyze in-reactor creep and swelling data obtained ca. 1977–1979 as part of the US breeder reactor program. The equations were developed according to the principles of incremental continuum plasticity for the purpose of analyzing data obtained from a novel irradiation experiment that was conducted, in part, using Type 304 stainless steel that had been previously irradiated to significant levels of void swelling. Analyses of these data support an earlier observation that all stress states, whether tensile, compressive, shear or mixed, can affect both void swelling and interactions between irradiation creep and swelling. The data were obtained using a set of five unique multiaxial creep-test specimens that were designed and used for the first time in this study. The data analyses demonstrate that the constitutive equations derived in Part I provide an excellent phenomenological representation of the interactive creep and swelling phenomena. These equations provide nuclear power reactor designers and analysts with a first-of-its-kind structural analysis tool for evaluating irradiation damage-dependent distortion of complex structural components having gradients in neutron damage rate, temperature and stress state.

Published by Elsevier B.V.

1. Introduction

An in-reactor multiaxial creep experiment was conducted ca. 1977–1979 in the Experimental Breeder Reactor (EBR-II) as part of the US breeder reactor development program [1]. Results of this "stress state" experiment, which was conducted in part using Type 304 stainless steel that had been previously irradiated to significant levels of void swelling, were summarized by Garner [2] in a review of the irradiation performance of fast reactor cladding and structural metals. However, details were not reported in the open literature due to reductions in funding and eventual cancellation of the US breeder reactor program. The data are reported and analyzed here using constitutive equations developed in a companion paper [3], which hereafter is called Part I.

Early results of the stress state experiment showed for the first time that any stress state, whether tensile, compressive, pure shear or a mixed stress state, may affect swelling. These results increased understanding of stress-affected swelling and the interaction of swelling with irradiation creep. As reviewed by Garner [2], a few early experiments were conducted using springs, beams and tensile specimens, but most stress effects experiments were conducted using pressurized tubes. The majority of these experiments showed that, providing the yield stress was not exceeded in-reactor, increasing stress levels progressively increased swelling, with later results demonstrating that the enhancement of swelling occurred primarily by shortening the duration of the transient regime.

Even though these experiments were conducted using specimens having both deviatoric and hydrostatic components of stress, it has been the practice to correlate stress-affected swelling for all stress states using empirical correlations that involved only the hydrostatic component of the stress state. Not only was the deviatoric component assumed to have no influence on swelling but such correlations predicted that compressive stresses would always produce lower swelling. These two rather significant conclusions were not examined experimentally until the late 1970s.

A deviatoric stress effect on swelling earlier had been predicted as a potential but small effect based on fundamental modeling of irradiation creep and swelling [4]. More recent irradiation creep modeling [5] also predicts that deviatoric stress may affect swelling and two additional experimental studies [6,7] reportedly have shown a deviatoric stress effect.

Constitutive equations capable of describing such effects were first proposed in 1979 by Hall [8]. Hall's early equations predicted

* Corresponding author. Tel.: +1 412 856 5347.
E-mail address: hallmm63@comcast.net (M.M. Hall Jr.).

0022-3115/$ - see front matter Published by Elsevier B.V.
doi:10.1016/j.jnucmat.2009.10.064

that the deviatoric and stress-affected swelling components each are functions of both deviatoric and hydrostatic components of stress, but only for non-linear creep and a mixed stress state having both deviatoric and hydrostatic stress components. These equations have been modified and extended in Part I so that stress-affected swelling may be a function of deviatoric stress for linear creep and in the absence of a hydrostatic component.

2. Multiaxial strain rate equations

Constitutive creep equations are derived in Part I by assuming an associated flow rule [9] for which the equivalent stress, σ_e, may serve as a plastic strain rate potential. Hall's original equivalent stress expression, which is a function of von Mises' invariant of the deviatoric stress, σ_{vM}, and the hydrostatic stress invariant, σ_H, was modified to include a term that couples these invariants. The resulting equation is

$$\sigma_e = \left\{\frac{2}{3}(1+\nu_p)\left[1+3\lambda(1-2\nu_p)\frac{\sigma_H}{\sigma_{vM}}\right]\sigma_{vM}^2 + 3(1-2\nu_p)\left[1+\frac{2}{3}\lambda(1+\nu_p)\frac{\sigma_{vM}}{\sigma_H}\right]\sigma_H^2\right\}^{\frac{1}{2}}, \quad (1)$$

where ν_p is the plastic Poisson's ratio and λ is the stress invariant coupling coefficient. One result of adopting this equation is that the stress invariants are no longer independent stress variables as the contribution of each to σ_e now depends on the magnitude of the other.

Plastic strain increment rates are obtained by partial differentiation of σ_e with respect to stress. The deviatoric creep rate components, $\dot{e}'_i$ $(i=1,2,3)$, are given by $\dot{e}'_i = \dot{\varepsilon}_e \partial\sigma_e/\partial\sigma'_i$ and the stress-affected swelling (volumetric creep) rate, $\dot{S}_\sigma$, is given by $\dot{S}_\sigma = \dot{\varepsilon}_e \partial\sigma_e/\partial\sigma_H$, where $\dot{\varepsilon}_e$ is the equivalent strain rate, σ'_i $(i=1,2,3)$ are the deviatoric stress components and σ_H is the hydrostatic stress. Note that the terms "stress-affected swelling" and "volumetric creep" are used here interchangeably depending on the context and desired emphasis. As discussed in Part I, the effective strain rate is taken to be $\dot{\varepsilon}_e \equiv \dot{\varepsilon}_o(\sigma_e/\sigma_o)^n$ where n is the stress exponent, $\dot{\varepsilon}_o$ is in principle any convenient reference strain rate and σ_o is a reference stress. For the case of swelling-independent creep, $\dot{\varepsilon}_o$ is related to the swelling-independent creep compliance, B_o, by $B_o = 3\dot{\varepsilon}_o/2\sigma_o$. For swelling-dependent creep, $\dot{\varepsilon}_o$ is taken as equal to the stress-free swelling rate, $\dot{S}_o$, and the creep-swelling coupling coefficient, D, is given by $D = (1+\nu_p)/\sigma_o$. By choosing for this case $\dot{\varepsilon}_o = \dot{S}_o$, deviatoric creep and swelling are strain-rate coupled phenomenologically, consistent with observations of "swelling-enhanced creep" [2]. Then the deviatoric and volumetric strain rate components are, respectively,

$$\dot{e}'_i = B_o\left(\frac{\sigma_e}{\sigma_o}\right)^{n-1}\sigma'_i + D\dot{S}_o\left(\frac{\sigma_e}{\sigma_o}\right)^{n-1}\left[2\lambda(1-2\nu_p)\sigma_H + \sigma'_i\right], \quad i=1,2,3, \quad (2)$$

and

$$\dot{S}_\sigma = \frac{3(1-2\nu_p)}{1+\nu_p}D\dot{S}_o\left(\frac{\sigma_e}{\sigma_o}\right)^{n-1}\left[\frac{2}{3}\lambda(1+\nu_p)\sigma_{vM} + \sigma_H\right]. \quad (3)$$

These equations show that, for all values n and as long as $-1 < \nu_p < 1/2$ and $\lambda > 0$, the deviatoric creep rate is a function of both the hydrostatic stress and the deviatoric stress and that the volumetric creep rate is a function of both the von Mises invariant of the deviatoric stress and the hydrostatic stress. Note that both $\dot{e}'$ and $\dot{S}_\sigma$ are asymmetric in stress, meaning that strain rates in tension are larger than rates in compression. The stress invariant coupling parameter, λ, and ν_p together determine the magnitude of the strain-rate coupling effect and the degree of asymmetry in stress dependency.

3. Experimental

3.1. Materials

Non-irradiated and previously irradiated annealed Type 304L stainless steel tubing sections having a nominal outer diameter of 7.63 mm, a nominal wall thickness of 0.51 mm and having the chemical composition shown in Table 1, were used in the manufacture of a set of five novel creep specimens, each providing a different stress state. Sections of non-irradiated and previously irradiation tubing also were produced for re-irradiation as stress-free swelling specimens.

Previously irradiated tubing was sectioned from capsules that had been used to encapsulate stainless steel-clad EBR-II fuel pins that were sodium-bonded and sealed in the Type 304L stainless steel capsules. The tubing sections selected for re-irradiation had been irradiated without applied stress at temperatures between 447 °C and 492 °C to initial fast neutron doses of 6.2–31.5 dpa. Twenty-seven stress-free controls and 29 stressed specimens were irradiated to higher fluence. The original irradiation plan for this experiment was for three re-irradiation cycles consisting of irradiation, extraction, measurement and reconstitution into a new irradiation vehicle. Unfortunately, decreases in funding allowed only one of these cycles to be completed.

3.2. Irradiation test vehicle

Test specimens were irradiated in Row 7 of EBR-II during reactor power runs 93A through 95H using a He gas-gapped, double-wall, hollow cylindrical test vehicle, shown schematically in Fig. 1. Five cylindrical specimen holders (tier cups) were stacked inside the irradiation test space, each holder having an inner diameter of 3.81 cm and a height of 7.62 cm. The test vehicle was contained within an outer hexagonal duct that guided the primary sodium coolant over the test vehicle outer wall. Thermal design [10] of the assembly called for heating the 371 °C inlet sodium to a maximum temperature of 510 °C, which, at the time the experiment was devised, was thought to be the peak swelling temperature of Type 304 stainless steel in the EBR-II fast neutron flux spectrum. The axial and radial distributions of irradiation temperature and neutron dose for three axial traces are shown in Figs. 2a and 2b. Note that the temperature peaks just above the mid-plane even though the coolant temperature rises with increasing height, reflecting primarily the higher gamma heating rate at mid-plane. The curves identified as "+0.65" and "−0.65" represent data obtained for test vehicle positions that, relative to the test vehicle centerline, are respectively 0.65 in. (1.65 cm) closer to and farther from the reactor core centerline. The curves marked as 0 represent data obtained for locations on the longitudinal axis of the test vehicle.

As shown in Fig. 2a, the measured temperature at the inlet to the irradiation test space was about 490 °C, which is comparable to the maximum irradiation temperature of the irradiated capsule material used to manufacture test specimens. The temperature rises to a maximum of about 560 °C at the axial mid-plane. Also

Table 1
Chemical composition of test specimens, wt.%.

Mn	P	S	Si	Ni	Cr	Ti	Cu	Mo	Co	C
1.66	0.016	0.014	0.59	10.6	18.3	<0.01	–	0.02	–	0.03

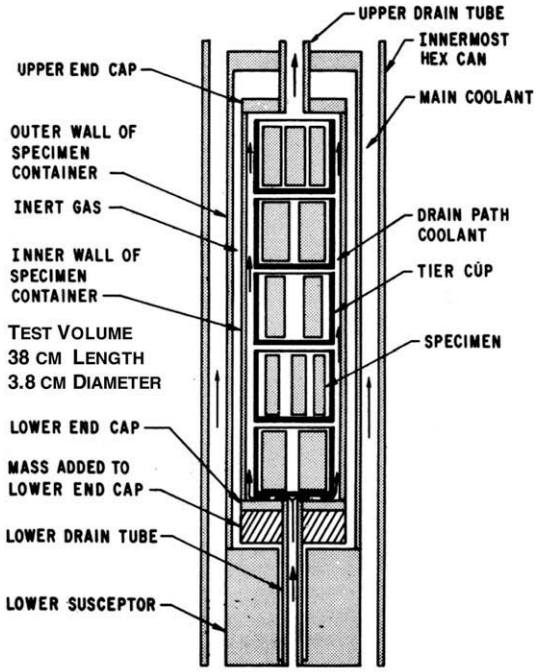

Fig. 1. Irradiation test vehicle. Elevated test temperatures were obtained using a helium gas-gapped double-wall insulated cylindrical specimen container to restrict loss of gamma heat.

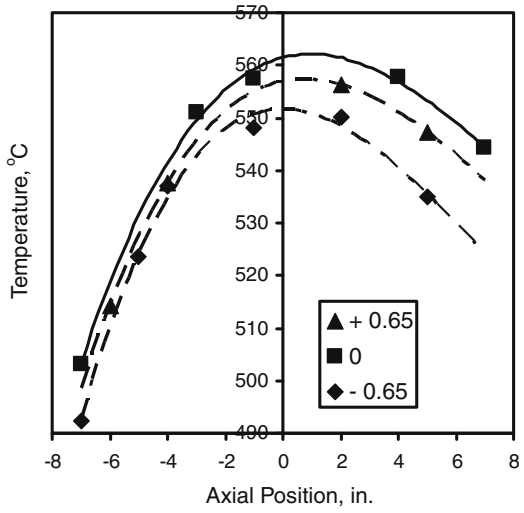

Fig. 2a. Axial and radial distributions of temperature within the irradiation test vehicle. Curves marked +0.65, 0, −0.65 represent temperatures at radial positions relative to the reactor core centerline.

shown in this figure is the radial temperature variation, which at the top of the irradiation test space was ~11 °C measured over the 3.3 cm distance from specimens closest to and most distant from the reactor core centerline. As shown in Fig. 2b, the measured axial distribution of neutron dose accumulated during the irradiation was from ~4.3 dpa at the bottom of the test space to a peak of about 6.6 dpa at the axial mid-plane. The radial damage variation was ~0.54 dpa or less over the 3.3 cm inner to outer specimen distance.

3.3. Test specimens

Special arrangements of bellows and tubing were used to manufacture the six stress state test specimens shown schematically in

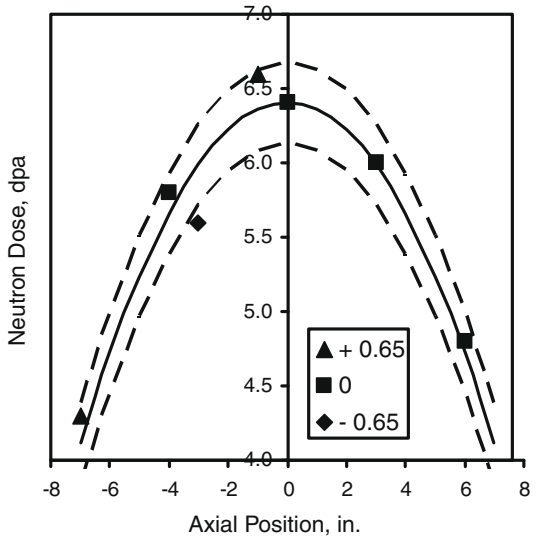

Fig. 2b. Axial and radial distributions of irradiation damage within the irradiation test vehicle. Curves marked +0.65, 0, −0.65 represent neutron dose at radial positions relative to the reactor core centerline.

Fig. 3. Test specimen design [11] and methods used in the fabrication and pressurization of these test specimens [12] have been reported previously. Five unique test specimen types were designed to attain three uniaxial and three biaxial stress states using internal pressurization and axial force loading of cylindrical tubing. Stress-free tubing sections were placed throughout the test vehicle to measure stress-free swelling for comparison to swelling of the stressed specimens. Longitudinal cross sectional views of these specimens are provided in Fig. 3. Uniaxial stress states include uniaxial compression aligned along the tubing length (0/−1), Fig. 3a, and uniaxial tension aligned either along the tubing length (0/1), Fig. 3b, or circumference (1/0), Fig. 3c. Biaxial stress states include circumferential-to-axial stress ratios of two-to-one (2/1), Fig. 3d, one-to-one (1/1), Fig. 3b, and one-to-minus-one (1/−1), Fig. 3e.

Table 2 lists the magnitudes of the test specimen stresses per unit internal pressure based on specimen and bellows dimensions. Effective applied stresses were in the range of 44 MPa to a maximum of about 180 MPa. No corrections were made for bellows stiffness as bellows were chosen to have low stiffness and irradiation creep relaxation of bellows walls was expected to further reduce the effective stiffness of each bellows. Non-irradiated prototypes of each specimen design were pressure and thermal creep tested ex-reactor to determine the pressure limits to ensure linear bellows behavior and to determine the capability of producing rational, multiaxial thermal-creep data.

3.4. Measurements

Neutron dose was determined post-test using neutron activation analyses of encapsulated fissile and non-fissile dosimeter materials. Dosimetry calculations were reported with an accuracy of about ±7%. Post-test immersion density measurements of Passive Thermal Expansion Difference temperature monitors, having an estimated accuracy of ±3 °C [13], were used to obtain temperature distributions with the irradiation test vehicle.

Swelling strain increments were determined for stress-free and stressed specimens from pre- and post-re-irradiation measurements of immersion density. Creep strain increments were determined for stressed specimens from pre- and post-re-irradiation measurements of tubing diameters and lengths. Multiple immersion density measurements of a non-irradiated Type 304 stainless

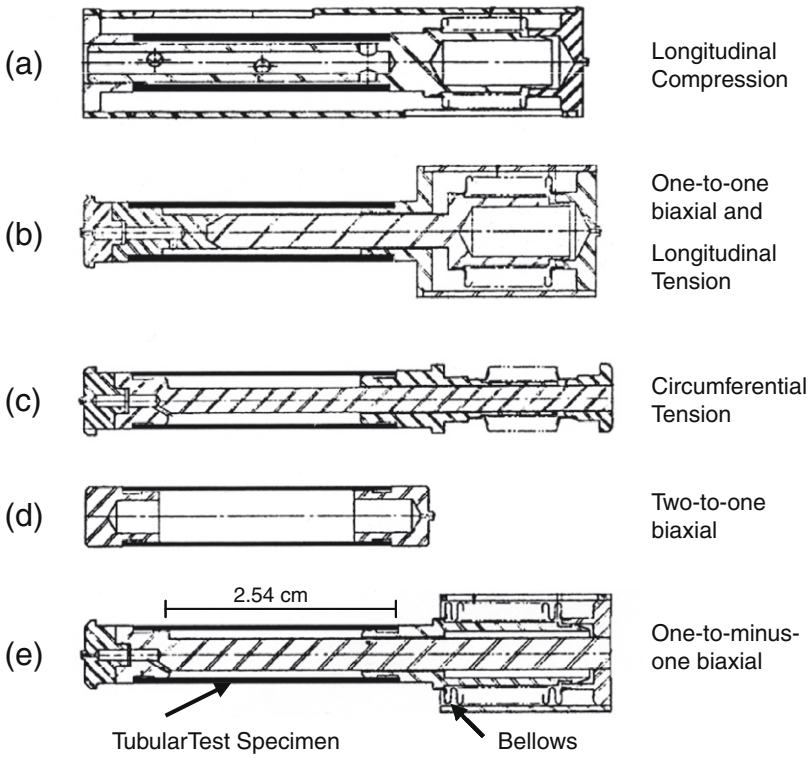

Fig. 3. Longitudinal cross sections of irradiation creep specimens. (a) 0/−1 longitudinal compression, (b) 0/−1 longitudinal and 1/1 biaxial tension, (c) 1/0 circumferential tension, (d) 2/1 biaxial tension and (e) 1/−1 shear.

Table 2
Stress magnitudes[a]/unit pressure.

Stress state[b]	σ_r/p	σ_θ/p	σ_z/p	σ_H/p	σ_{vM}/p	σ_H/σ_{vM}
0/1	0	0	10.41	3.470	10.410	0.33
0/−1	0	0	−10.41	−3.470	10.410	−0.33
1/0	−0.5	6.865	0.297	2.221	7.001	0.32
2/1	−0.5	6.865	3.4325	3.266	6.383	0.51
1/−1	−0.5	6.865	−6.977	−0.204	11.996	−0.02
1/1	−0.5	6.865	6.659	4.341	7.264	0.60

[a] Mid-wall stress.
[b] Nominal ratio of circumferential to longitudinal stresses.

steel standard, having a nominal density of 7.8977 gm/cc, produced a two sigma variation of 0.0028 gm/cc, 0.035% of the nominal density. The pre-irradiated specimens were found to have somewhat larger diametral variation due to interaction with the wire wraps that separated the cladding and capsule. The typical variation of diameters measured every 20° at each of four axial positions was 0.072 mm, 0.94% of each local average, while the axial variation in the local average diameters was typically 0.0063 mm, 0.082% of the axial average. Length measurements were made using prepositioned micro hardness indentions. Multiple length measurements of a standard specimen having a nominal standard length of 1.35 cm, showed a two sigma variation of 0.00077 cm, 0.057% of the nominal length, and a data range of 0.00135 cm, 0.10% of the nominal length.

Typical two sigma variations in strain measured on irradiated test specimens are 0.016 diametral strain, 0.00081 length strain and 0.00049 swelling strain. For comparison, the maximum measured strains were 0.013 diametral strain, 0.012 length strain and 0.029 swelling strain. Based on these comparisons, considerable data scatter is expected for data correlations derived from diametral strains while somewhat less scatter can be expected for data correlations involving length and swelling strains only.

4. Results

4.1. Stress-free swelling

Pre- and post-test strains and rates for the stress-free specimens are provided in Table 3. Fig. 4 shows stress-free swelling strains derived from these data plotted versus neutron dose for each of the 27 stress-free control specimens in the initial irradiation condition. These specimens each were irradiated initially within one of three relatively narrow temperature ranges, 445–456 °C, 470–475 °C and 486–492 °C. Information regarding dose rates associated with each of these temperature ranges is no longer available. However, it is likely that a range of dose rates are associated with each temperature range. At the time the stress state experiment was designed the practice was to treat dose as the irradiation damage variable and to select specimens based on an assumption that there was but a small effect of dose rate on irradiation creep and swelling for the range of dose rates associated with the stress state experiment.

A test objective served by Fig. 4 was to select test materials having an irradiation history that would not obscure interpretation of the re-irradiation test results. For example, examination of Fig. 4 shows that any apparent effect of temperature in the temperature range 445–492 °C is small so that the data set can be considered internally independent of temperature history. Furthermore, the stress-free swelling rate (slope of the linear curve drawn through the data) can be considered nearly constant and independent of dose for a neutron dose greater than an "incubation" or "transient" dose [14] of about 13.5 dpa ($\sim 3 \times 10^{22}$ n/cm^2, $E > 0.1$ MeV).

Note that the "steady-state" swelling rate for a dose above 13.5 dpa is only about one-half of the 1%/dpa steady-state swelling rate found to be characteristic of all 300 series stainless steels over a temperature range that includes the range of irradiation and re-irradiation temperatures in this test [2]. The 1%/dpa rate has also

Table 3
Stress-free specimens: pre- and post-re-irradiation swelling strains and rates.

ID	Location axial-radial		Dose rate (10^{-7} dpa/s)	Initial dose (dpa)	Δ dpa	Initial T (°C)	Final T (°C)	Initial swelling strain	Final swelling strain	$\Delta S_o/\Delta$ dpa (10^{-3}/dpa)
High dose specimens										
11	−7.13	0.65	2.29	28.4	3.76	454	489	0.0716	0.0909	4.793
118	−7.13	0.00	2.46	29.1	4.03	492	501	0.0823	0.1077	5.825
114	−7.13	0.39	2.56	31.7	4.19	472	500	0.0932	0.1185	5.536
117	−6.38	0.00	2.75	33.1	4.50	470	514	0.0939	0.1149	4.261
18	−6.38	0.39	2.84	19.8	4.66	473	513	0.0308	0.0488	3.749
110	−5.63	0.39	3.10	31.9	5.09	445	524	0.0802	0.0909	1.934
112	−4.13	0.00	3.42	22.0	5.61	489	543	0.0417	0.0601	3.152
15	−3.38	0.00	3.58	21.1	5.87	475	549	0.0387	0.0570	3.000
12	−2.63	0.65	3.87	22.2	6.35	474	548	0.0601	0.0754	2.268
111	−1.13	0.65	4.03	26.1	6.62	473	555	0.0681	0.0851	2.396
17	−0.38	0.00	3.90	25.4	6.40	454	561	0.0520	0.0573	0.782
14	0.38	0.00	3.90	27.0	6.40	456	562	0.0630	0.0701	1.054
19	1.88	0.00	3.81	16.3	6.24	488	560	0.0120	0.0201	1.289
13	3.38	0.65	3.75	18.4	6.14	486	551	0.0160	0.0282	1.954
116	4.88	0.65	3.39	34.1	5.56	447	546	0.0852	0.0925	1.214
113	5.63	0.65	3.17	33.8	5.19	451	543	0.0899	0.0981	1.446
16	6.38	0.00	2.75	17.5	4.50	487	546	0.0162	0.0276	2.503
115	6.38	0.00	2.75	27.5	4.50	491	546	0.0752	0.0968	4.448
Low dose and initially non-irradiated specimens										
119	−3.38	0.65	3.75	8.2	6.14	472	544	0.0064	0.0153	1.436
120	2.68	0.00	3.70	7.0	6.07	490	559	0.0028	0.0071	0.706
121	1.88	0.65	3.97	7.4	6.51	473	555	0.0046	0.0086	0.614
122	−0.38	0.65	4.07	6.3	6.67	490	556	0.0018	0.0054	0.527
123	6.38	0.00	2.75	0.0	4.50	NA	546	0.0000	0.0011	0.262
124	2.63	0.65	3.87	0.0	6.35	NA	553	0.0000	0.0022	0.244
125	−7.13	0.39	2.56	0.0	4.19	NA	500	0.0000	0.0024	0.548
126	−4.13	0.00	3.42	0.0	5.61	NA	543	0.0000	0.0016	0.206
127	−1.13	0.00	3.87	0.0	6.35	NA	560	0.0000	0.0015	0.262

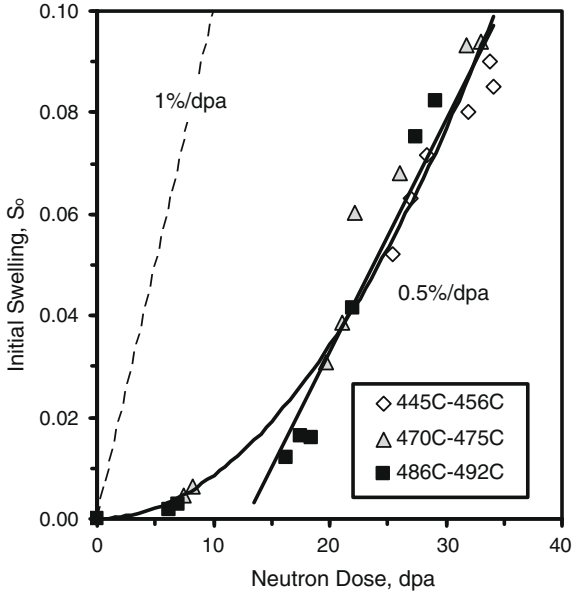

Fig. 4. Initial swelling strains measured for Type 304 stainless steel stress-free control specimens which were irradiated in the temperature range 445–492 °C. A derived quasi-steady-state swelling rate of ~0.5%/dpa indicates either that anticipated steady-state swelling rate of 1%/dpa has not been attained or has been obscured by dpa rate variations in the data.

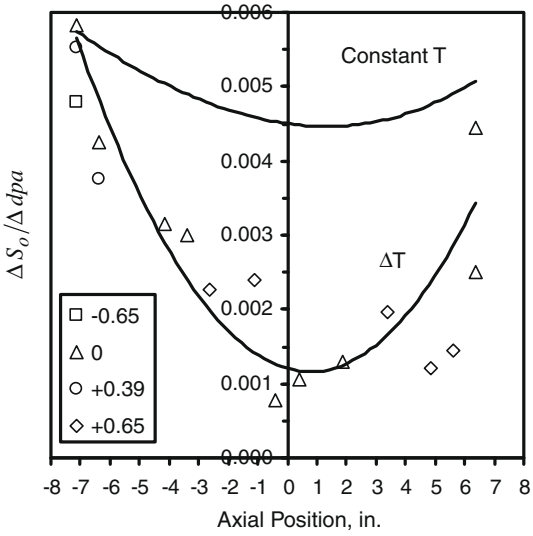

Fig. 5. Re-irradiation swelling rate for stress-free specimens re-irradiated at higher temperatures and at multiple elevations in the irradiation test vehicle. Shown for comparison is the predicted swelling rate for specimens not subject to a temperature change.

been shown to be characteristic of 304 stainless steel, although the transient regime is somewhat more curvilinear in this easily swelling steel, compared to more swelling-resistant steels [15,16].

It may be that the irradiated specimens having damage levels greater than 13.5 dpa have not yet achieved steady-state swelling as it has been demonstrated recently that dose rate variations within a data set potentially characteristic of this experiment will produce the appearance of a lower steady-state swelling rate due to progressive shortening of the transient regime at lower dpa rates [17–19]. However, for the relatively small re-irradiation dose increments in this test, it may be assumed that a quasi-steady-state has been attained. Normalization of re-irradiation swelling strain increments by the re-irradiation neutron dose increment will then give instantaneous swelling rates that are relatively independent of dose increment. Data obtained from specimens having an initial irradiation dose of less than 13.5 dpa were not

analyzed for stress state effects as there was insufficient additional swelling strain to provide reliable measurements of strain increments.

Increments in stress-free swelling, ΔS_o, were divided by the increments in neutron dose, Δ dpa, and plotted versus axial position in the irradiation test vehicle, Fig. 5. Shown for comparison is the predicted axial distribution of swelling rates for capsule material irradiated without temperature change [14,20]. Comparison with the re-irradiation swelling data clearly shows that there is an effect of reirradiating specimens at a temperature above the initial irradiation temperature. Fig. 6 shows that there is a linear decrease in the swelling rate of about an order of magnitude as the temperature change increases from 10 °C to 110 °C. Note that, as only one of three originally planned re-irradiation cycles was conducted, neutron dose and dose rate effects are not easily separable. Moreover, as shown in Fig. 7, the effects of neutron dose and temperature cannot be separated easily as neutron flux and irradiation temperature are axial co-variables below the test vehicle centerline and deviating significantly only at the uppermost elevations above the centerline.

Fig. 6 shows that there is reasonably good correlation ($R^2 = 0.87$) of stress-free re-irradiation swelling rate with temperature change (re-irradiation temperature minus original irradiation temperature). Other correlations that were attempted, but showed less correlation, include swelling rate with dose increment ($R^2 = 0.64$), re-irradiation temperature ($R^2 = 0.68$) and initial swelling strain ($R^2 = 0.11$). However, as the swelling strain rate derived from the data in Fig. 4 likely has not attained steady-state, the swelling rate should retain some dependence on the instantaneous swelling strain. To test this possibility, while accepting the apparent strong dependence on temperature change, the data were fit to an empirical correlation equation having the form

$$\Delta S_o/\Delta \text{ dpa} = (a_o + a_1 \Delta T) S_o^n. \quad (4)$$

A better fit of the data is attained ($R^2 = 0.95$) using this correlation, as shown in Fig. 8. The swelling exponent of $n = 0.25$ indicates, as expected, that there is a weak dependence of the swelling rate

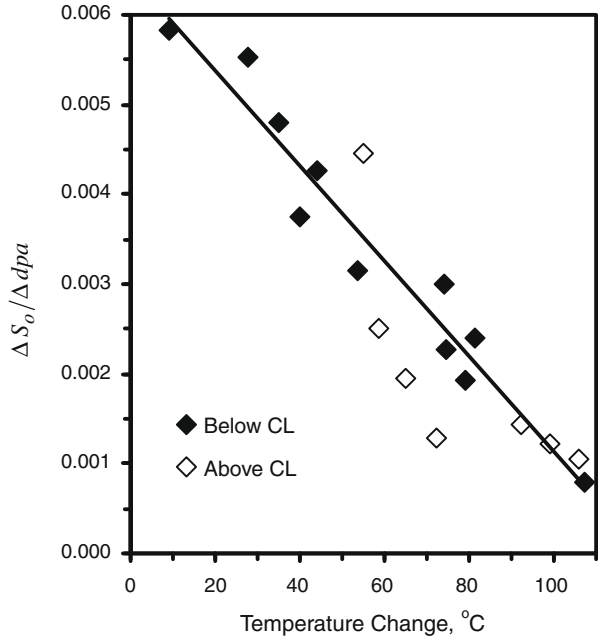

Fig. 6. Re-irradiation swelling rate for stress-free specimens as a function of temperature change. A decrease in swelling rate with increasing change in temperature is clearly observed.

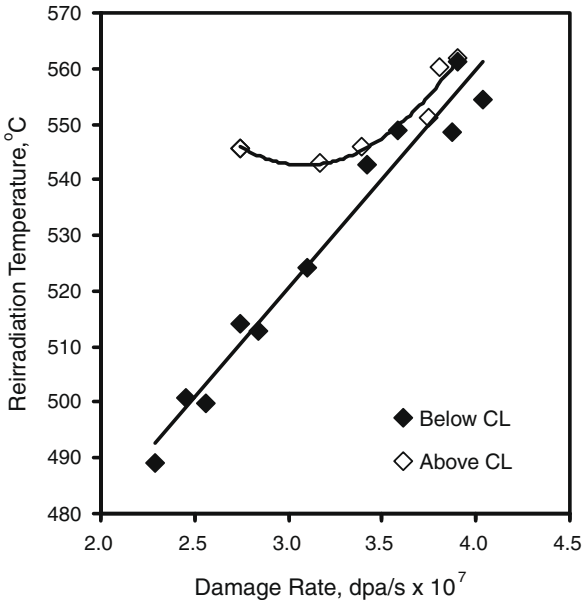

Fig. 7. Correlation between re-irradiation temperature and irradiation damage rate within the irradiation test vehicle. Effects of temperature and damage rate cannot be separated as irradiation temperature and damage rate are co-variables for all elevations except the top most locations.

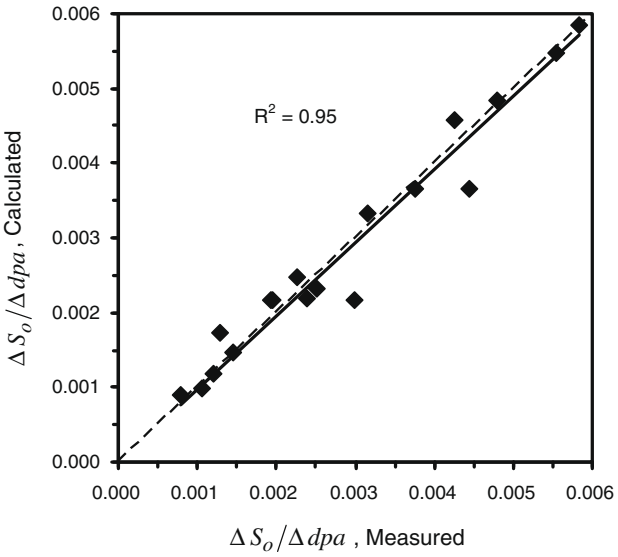

Fig. 8. Re-irradiation swelling rate, calculated using Eq. (4), versus the measured re-irradiation swelling rate. The re-irradiation swelling rate is an apparent function of the temperature increase, and to a lesser extent, the initial swelling strain.

on the initial swelling strain for these higher fluence specimens. Eq. (4) was used to calculate the stress-free swelling expected for each of the stressed specimens.

4.2. Stress-affected swelling

Pre-test and re-irradiation specimen conditions for the stressed specimens are provided in Table 4. Pre- and post-test swelling, length and diametral strains for these specimens are provided in Table 5. Of the eighteen stressed specimens having an initial dose of greater than 13.5 dpa, four specimens developed leaks, thus losing pressure at some undefined time during the irradiation

Table 4
Stressed specimens: pre- and re-irradiation specimen conditions.

Type	ID	Location axial-radial		Dose rate (10^{-7} dpa/s)	Initial dose (dpa)	Δ dpa	Initial T (°C)	Final T (°C)	$P(T)$ (MPa)	von Mises stress (MPa)	Hydro-static stress (MPa)
High dose specimens											
1/−1	21	7	−0.3	2.43	26.1	3.99	459	535.5	12.28	147.3	−2.50
1/−1	22	−2	0.0	3.79	22.5	6.22	486	551.7	4.44	53.3	−0.91
1/−1	23	4	−0.3	3.37	20.0	5.53	489	546.6	4.42	53.0	−0.90
2/1	31	4	0.0	3.45	23.3	5.66	475	549.2	9.41	60.1	30.74
2/1	32	−6	0.0	2.88	21.1	4.72	438	514.7	17.83	113.8	58.24
0/1	42	−2	0.3	3.87	22.6	6.34	489	554.4	5.48	57.0	19.00
0/1	43	2	0.3	3.87	19.0	6.34	490	557.5	5.50	57.2	19.07
1/0	62	−4	0.0	3.45	29.3	5.66	460	538.5	21.20	148.4	47.08
0/−1	51	5	−0.3	3.12	30.2	5.11	490	542.9	14.63	152.3	−50.76
0/−1	52	4	−0.3	3.37	28.0	5.53	463	546.6	5.42	56.5	−18.82
0/−1	53	−4	−0.3	3.37	23.7	5.53	497	535.9	5.35	55.7	−18.57
0/−1	55	−5	−0.3	3.12	25.1	5.11	490	525.4	10.40	108.3	−36.09
1/1	71	5	0.3	3.27	33.6	5.36	455	548.3	12.00	87.1	52.08
1/1	72	−4	0.3	3.53	30.7	5.78	481	541.2	6.05	43.9	26.27
2/1	36[a]	7	−0.6	2.36	21.4	3.86	453	532.8	24.29	155.0	79.32
2/1	38[a]	7	0.3	2.58	27.0	4.24	465	540.9	17.58	112.2	57.40
1/0	61[a]	5	0.0	3.19	32.8	5.24	470	545.6	21.39	149.7	47.49
0/1	41[a]	5	0.3	3.27	24.8	5.36	465	548.3	14.72	153.3	51.09
Low dose and initially non-irradiated specimens											
0/−1	24	4	0.3	3.53	7.4	5.78	480	551.9	8.91	64.7	38.67
2/1	34	−2	−0.3	3.72	6.7	6.09	480	549.0	24.62	178.9	106.90
0/−1	25	1	−0.3	3.80	0.0	6.23	NA[b]	553.6	8.93	64.8	38.75
0/−1	26	−5	0.3	3.27	0.0	5.36	NA	530.7	8.68	63.0	37.68
2/1	35	1	−0.6	3.73	0.0	6.11	NA	550.9	18.65	135.5	80.98
0/1	44[a]	1	0.3	3.95	0.0	6.48	NA	558.9	10.84	78.7	47.05
0/−1	54	1	−0.3	3.80	0.0	6.23	NA	553.6	10.77	78.2	46.75
1/0	63	1	0.0	3.88	0.0	6.36	NA	556.2	15.69	114.0	68.13
1/1	73	−1	0.3	3.95	0.0	6.48	NA	557.6	12.13	88.1	52.67

[a] Leaker.
[b] Not applicable.

Table 5
Stressed specimens: swelling, length and diametral strain increments.

Type	ID	Initial swelling strain	Final swelling strain	$\Delta L/L$	$\Delta D/D$	$\Delta S/\Delta dpa$	$\Delta S_\sigma/\Delta S_o$	$\Delta e'_L/\Delta S_o$	$\Delta e'_D/\Delta S_o$
High dose specimens									
1/−1	21	0.0683	0.0793	−0.00153	0.00822	0.00275	0.3717	−0.6484	0.5701
1/−1	22	0.0479	0.0650	0.00332	0.00800	0.00275	0.0805	−0.1541	0.1479
1/−1	23	0.0290	0.0454	0.00382	0.00699	0.00296	0.1644	−0.1141	0.1070
2/1	31	0.0468	0.0634	0.00555	0.00741	0.00294	0.4623	0.0001	0.1637
2/1	32	0.0393	0.0593	0.00690	0.01001	0.00425	1.4693	0.0263	0.4094
0/1	42	0.0488	0.0716	0.01074	0.00411	0.00360	0.3861	0.1900	−0.2125
0/1	43	0.0272	0.0447	0.00937	0.00335	0.00276	0.2852	0.2600	−0.1823
1/0	62	0.0863	0.1155	0.00796	0.02118	0.00517	1.4688	−0.15101	0.9640
0/−1	51	0.0829	0.0882	−0.01068	0.00352	0.00102	−0.7096	−0.6892	0.0986
0/−1	52	0.0787	0.0874	0.00073	0.00319	0.00157	−0.1044	−0.2233	0.0303
0/−1	53	0.0557	0.0769	0.00296	0.00595	0.00384	−0.0271	−0.1888	−0.0515
0/−1	55	0.0716	0.0891	−0.00218	0.00000	0.00344	−0.2027	−0.2197	−0.1210
1/1	71	0.0921	0.1079	0.00851	0.00601	0.00295	1.2682	0.4499	0.1032
1/1	72	0.0908	0.1172	0.00768	0.00965	0.00457	0.4005	−0.0596	0.0446
2/1	36[a]	0.0447	0.0544	0.02699	0.00399	0.00253	0.5261	4.23993	0.1147
2/1	38[a]	0.0894	0.0990	0.00248	0.00431	0.00228	0.0549	−0.0115	0.1187
1/0	61[a]	0.0939	0.1080	0.00582	0.00503	0.00271	0.2030	−0.1352	0.0256
0/1	41[a]	0.0566	0.0708	0.00864	0.00822	0.00264	0.6435	NA	−0.3706
Lose dose and initially non-irradiated specimens									
0/−1	24	0.0039	0.0104	−0.00086	0.00366	0.00112	[b]	[b]	[b]
2/1	34	0.0034	0.0092	0.00227	0.00456	0.00094	[b]	[b]	[b]
0/−1	25	0.0000	0.0015	0.00026	0.00076	0.00020	[b]	[b]	[b]
0/−1	26	0.0000	0.0024	–	0.00221	0.00045	[b]	[b]	[b]
2/1	35	0.0000	0.0023	0.00089	0.00186	0.00040	[b]	[b]	[b]
0/1	44[a]	0.0000	0.0024	0.00201	−0.00066	0.00034	[b]	[b]	[b]
0/−1	54	0.0000	0.0016	−0.00101	0.00028	0.00029	[b]	[b]	[b]
1/0	63	0.0000	0.0030	0.00034	−0.00003	0.00045	[b]	[b]	[b]
1/1	73	0.0000	0.0020	0.00059	0.00062	0.00032	[b]	[b]	[b]

[a] Leaker.
[b] Length, diameter and stress-free density changes too small to compute meaningful strain increments.

period and consequently these specimens are not used in the data analysis. Data obtained on these latter specimens are included in Table 5 but are segregated in a separate section of the table.

Fig. 9a shows swelling rates for stressed specimens compared to unstressed specimens plotted versus elevation within the irradiation test space. These data show that in most cases the stressed

specimen swelling rates exceed the stress-free swelling rates. Fig. 9b provides a better comparison by showing measured swelling rate increments for surviving stressed specimens plotted versus calculated stress-free swelling rate increments, Eq. (4), corresponding to each of the stressed specimens. This figure shows that measured swelling increments obtained on stressed specimens were less than calculated stress-free swelling increments for only four specimens while for all others measured swelling increments were greater than corresponding stress-free swelling values. The four specimens showing a negative stress effect on swelling are all uniaxial compression specimens designated as 0/−1. These are the only test specimens that had a compressive hydrostatic stress component. For all other stress states, including the pure shear stress state, (1/−1), swelling rate increased relative to the stress-free specimens. Of the four compression test specimens, the lower stressed specimens had a small negative effect on swelling while the two more highly stressed specimens had larger negative swelling rates.

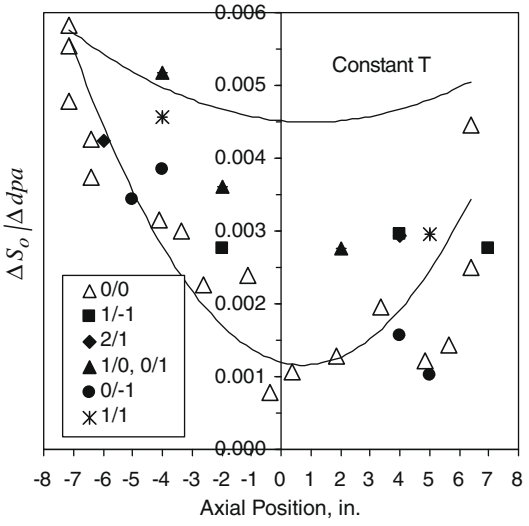

Fig. 9a. Swelling rates observed for both stress-free and stressed specimens as a function of axial position in the test vehicle. Solid symbols denote stressed specimens and open symbols denote unstressed specimens.

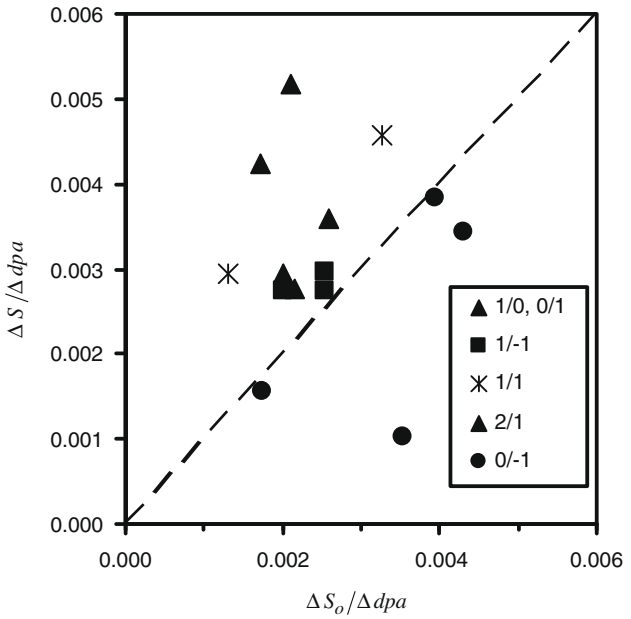

Fig. 9b. Swelling rate observed for stressed specimens versus swelling rate predicted for stress-free specimens. Symbols above the dashed line indicate that the applied stress increased the swelling rate while those below the line indicate that stress reduced the swelling rate.

Figs. 10 and 11 show normalized stress-affected swelling plotted, respectively, as a function of the hydrostatic and von Mises invariants of stress. The curves in these figures represent fits of the data to Eq. (3) for constant ratios of the hydrostatic and von Mises invariants of each stress state. Data obtained using the biaxial 1/−1 pure shear specimens, shown in Fig. 10, confirm that there is a deviatoric stress effect in the absence of a hydrostatic stress component. Fig. 11 emphasizes this result by showing that volumetric strain rate can be correlated with deviatoric stress for all stress states tested. Data obtained using the uniaxial 0/−1 and 0/1 specimens show that the effect of both hydrostatic and deviatoric stress is asymmetric, meaning that strain rates in tension are greater in magnitude than the negative strain rates in compression. Fitting the stress-affected swelling data to Eq. (3), and using Eq. (1), gives best-fit values for the equation parameters: $n = 1.66$, $\nu_p = 0.095$, $\lambda = 0.180$ and $\sigma_o = 127.9$ MPa. Results of the regression analysis, Fig. 12, show that the fit is excellent as $R^2 = 0.99$.

4.3. Deviatoric creep

Fig. 13 shows the length and diametral increments in deviatoric creep strain, normalized by the calculated stress-free swelling strain increment and plotted as a function of the deviatoric stress component. As expected, the diametral deviatoric strain shows considerable scatter due to the previously mentioned greater uncertainty inherent in the measurements of diameter. The curves in this figure were drawn using Eqs. (1) and (2) and using the best-fit parameters that were determined by fitting the volumetric strain increment data. Note that in using Eq. (2) for this purpose, the swelling-independent creep coefficient, B_o, was set equal to zero as the specimens needed to obtain estimates of B_o, that is, those having initial zero or low fluences did not provide measurable length and diameter strains for the one irradiation period that was conducted. As shown in Fig. 14, the fit to the length strain data

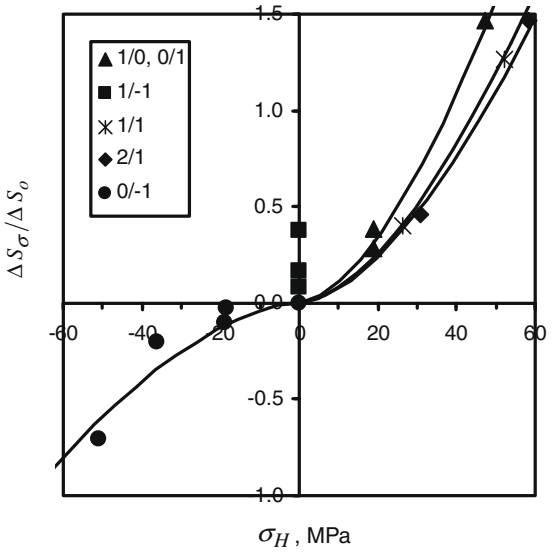

Fig. 10. Normalized stress-affected swelling versus hydrostatic stress. Measurable swelling for the 1/−1 shear stress state specimens shows that deviatoric stress may affect swelling in the absence of a hydrostatic stress component. Curves represent calculations using Eq. (3).

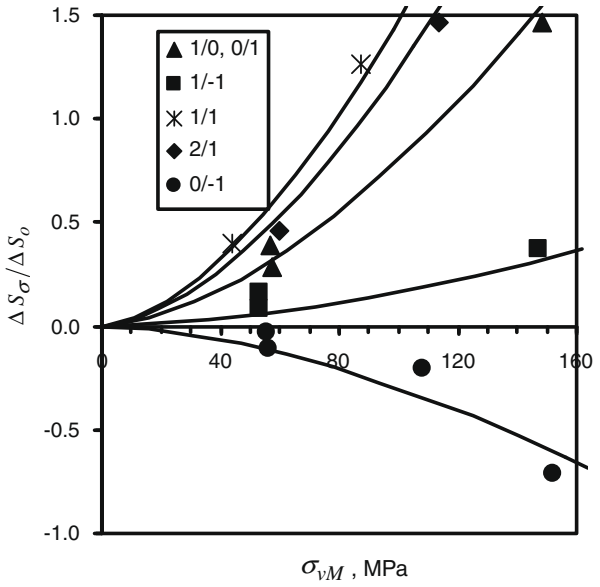

Fig. 11. Normalized stress-affected swelling versus the von Mises invariant of deviatoric stress. When plotted versus the von Mises invariant all the data can be compared to predictions of the constitutive equations. Curves represent calculations using Eq. (3) and the stress ratios found in Table 2.

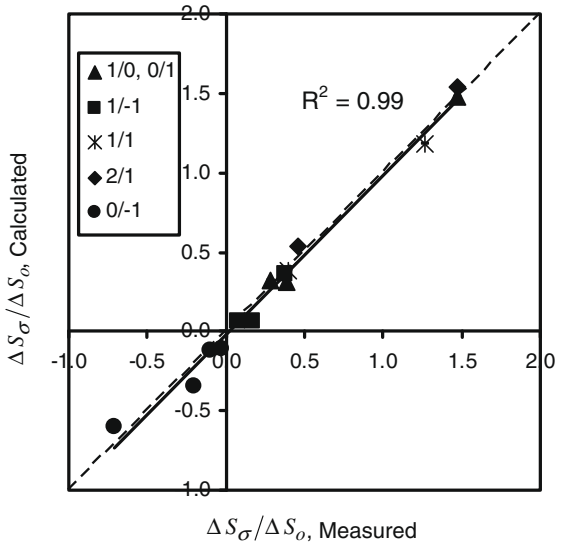

Fig. 12. Normalized stress-affected swelling rate calculated using Eq. (3) versus the measured normalized values of stress-affected swelling. The excellent correlation between calculated and measured rates indicates very consistent data and strongly validates the derived constitutive equations.

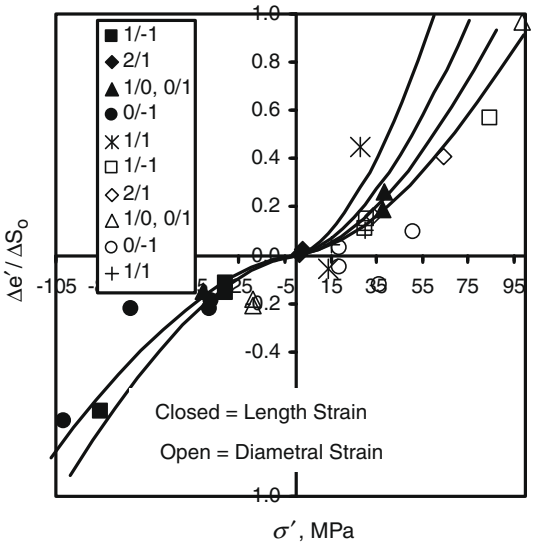

Fig. 13. Normalized deviatoric creep rate versus deviatoric stress. Curves represent calculations using Eq. (2) and the best-fit parameters obtained by fitting the stress-affected swelling data to Eq. (3).

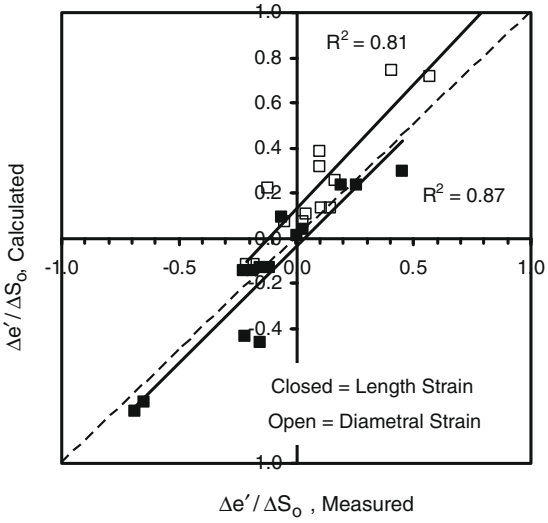

Fig. 14. Normalized deviatoric creep rate calculated using Eq. (2) versus the measured normalized values of the deviatoric creep rate. Larger measurement uncertainties in length and diametral strains account for the somewhat inferior correlations, R^2, of these data.

is reasonable, having an R^2 of 0.87. However, as expected, the fit to the diametral data is not quite as good, having an R^2 of 0.81.

5. Discussion

Our ability to isolate and quantify the effects of stress state on irradiation creep and swelling potentially is confounded by the apparent temperature history effect seen in Figs. 5 and 6. This situation is complicated further by coupling of temperature and dose rate effects by the re-irradiation test vehicle design. The observed effect of an increase in temperature on stress-free swelling rate is an unexpected result and is not understood within context of the current understanding of irradiation creep and swelling. Phenomenological evidence for the effects of temperature history on swelling has been summarized by Garner [2], who finds the phenomena to be complex, depending strongly on alloy composition and starting condition, the nature of the microchemical evolution that precedes and accompanies swelling, and depending on whether the steady-state swelling rate was reached prior to the temperature change. The situation is as equally complicated theoretically as conventional rate theory models of void nucleation and growth are not directly relevant to the swelling-before-creep data obtained in this experiment.

The analysis method used here to isolate stress state effects is to normalize both deviatoric creep and stress-affected swelling (volumetric creep) components by the stress-free swelling rate. The assumption implied by this method is that these creep components are simply proportional to the stress-free swelling rate and that any history effects that may be due to changes in temperature

and dose rate are carried entirely by the stress-free swelling. As mentioned above, the swelling-independent deviatoric creep, if there is any present, could not be obtained due to data limitations. Given the one irradiation period of this experiment, validity of model can be judged only by the ability of the constitutive law developed in Part I to faithfully represent the stress state effects revealed by this method.

A potentially useful result of the constitutive equation development of Part I and the data analysis here is that the deviatoric creep rates were well predicted using the equation parameters derived by fitting only the swelling rate data. This result means that a complete constitutive description potentially may be obtained using a limited number of stress states, for example, longitudinal tension, compression and biaxial tension (capped-end pressurized tubes) and by making only immersion density measurements, avoiding the added difficulty and lower accuracy of length and diameter measurements. Note that the ability to do this depends on either the swelling-independent deviatoric creep rate being small in comparison to the swelling-dependent deviatoric creep rate or that swelling-independent creep be obtainable from low swelling (low dose) creep specimens.

The importance of the plastic Poisson's ratio, ν_p, relative to stress and stress state effects on creep and swelling has been discussed in some detail in Part I and by Wire and Straalsund [21]. The discussion in Part I focuses on the fact that deviatoric and volumetric creep components are coupled by their mutual dependence on stress-free swelling and that the magnitudes of ν_p and the stress invariant coefficient λ determine the relative magnitudes of each creep component. With increasing irradiation exposure the irradiation-induced microstructure becomes increasingly dominated by the void fraction and, as a consequence, ν_p decreases from a maximum value of 1/2, which is characteristic of non-irradiated metals and for which creep is entirely volume-conservative, deviatoric creep. As the void fraction increases, ν_p decreases and the volumetric component increases at the expense of the deviatoric component. For experiments involving significant swelling these stress effects become measurable. For example, in this experiment where void volumes exceed 6%, ν_p is reduced to 0.095 and the volumetric creep in a uniaxial creep test exceeds the deviatoric creep rate by about 35%. However, experiments having low dose irradiation exposures, for which the swelling is less than say 2%, the magnitude of both the volumetric creep (stress-affected swelling) rate, Eq. (3), and the hydrostatic stress-affected deviatoric creep rate, Eq. (2), are less than about 10% of the deviatoric creep rate. In the experiment of Sahu and Jung [6] where swelling was less than ~0.4%, the stress-affected swelling is expected to be less than 2% of the deviatoric creep. For an effect this small, it is unlikely that any difference in either creep or swelling would be detected when comparing the effect of tensile versus compressive stresses. For these reasons, low dose experiments cannot provide conclusive evidence regarding the potential influence of stress state on either deviatoric creep or stress-affected swelling.

Conclusions regarding stress state effects on irradiation creep and swelling have been drawn in the past from results obtained using beams in bending [22] and dead weight loading of helical springs has been used to obtain near pure shear stress states for irradiation creep experiments. A problem with both these types of creep specimens is that they have large stress gradients through their cross sections. The pressurized thin-wall tube with axial force loading used here has a much smaller radial stress gradient across the tube wall. The stress in a beam goes from tension to compression when traversing the beam thickness and the spring torsion stress goes from zero at the center to a maximum at the outer fiber of the spring wire cross section. This is not a problem for either beams or springs when the initial stress loading is linear elastic, creep is linear in stress, creep rates in tension and compression are equal and swelling strains are uniformly distributed across section. However, when any one of these requirements is not met, stress distributions are no longer linearly distributed and internal stresses build up in complex patterns that cannot be predicted using the simple beam and torsion stress equations that are usually applied to the analyses of these experiments. Stress effects on swelling can be offset due to the simultaneous effects of tension and compression for the bent beam specimen and displacement of the neutral beam axis can affect beam deflection rates in complex ways. The thin-wall tube specimens used in this test have a radial gradient in stress of plus and minus 7.5% about the midwall stress used in the data analysis. So long as these tubes have concentric inner and outer diameters, the effect of stress redistribution across the tube wall has no effect on axial stresses and the effect of the midwall circumferential stress is small.

6. Conclusions

The results of this study support the following conclusions:

1. Normalization of the deviatoric creep and stress-affected swelling data by the stress-free re-irradiation swelling rate is effective in revealing stress state effects. Comparisons of the normalized data to the constitutive equations developed in Part I show that these equations capture the complex behaviors that are evident in the deviatoric and volumetric creep data.
2. Equation parameters are comparable to those derived from rate theory models and conventional pressurized tube creep data obtained without a temperature change history. A value for ν_p of 0.095 is reasonably consistent with that expected based on the work by Straalsund et al. [4] who estimated that $\nu_p = 0.02$ for stainless steel irradiated to approximately 20 dpa (compares to ~ 25–40 dpa in this test) in the temperature range of ~450 °C to ~550 °C. Straalsund based his estimate on a microstructural model, for which creep is linear in stress (compares to $n = 1.66$ in this test), and on measurements of irradiation void size, void density and dislocation density.
3. A value of 127.9 MPa for the reference stress, σ_o, falls midway between the intrinsic dislocation creep stress (~96 MPa) and the dislocation-glide stress (168 MPa) that were used by Zinkle and Lucas [23] to construct deformation mechanism maps for irradiated Type 316 austenitic stainless steel. This is consistent with a non-linear ($n = 1.66$), climb-enabled dislocation-glide mechanism of creep.
4. Magnitudes of these parameters are consistent with the magnitude of the so-called "creep-swelling coupling coefficient", D, derived by Toloczko and Garner [24] for the case where stress-free swelling is used in the creep-swelling coupling expression. They found that $D = 0.0060\ \text{MPa}^{-1}$ which compares well with the value of $D = 0.0086\ \text{MPa}^{-1}$ that was derived here using $D = (1 + \nu_p)/\sigma_o$ and substituting the parameter values obtained here.
5. Phenomenologically, the results of this experiment can be described as follows:
   a. Deviatoric creep and stress-affected swelling are each dependent on both deviatoric and hydrostatic components of stress.
   b. Stress-affected swelling may occur for pure shear stress states for which there is only a deviatoric stress and no hydrostatic stress component. This implies that the interpretation of early helical spring experiments, which involve pure deviatoric stresses, may have been confounded by stress-affected swelling.

c. Although pure hydrostatic stress states are not common for reactor structural components, the constitutive law developed here predicts that deviatoric creep may occur for pure hydrostatic stresses. However, mechanistically this would require that there be a preexisting anisotropic distribution of dislocation Burgers vectors.
d. Stress states having a compressive hydrostatic stress component, such as the longitudinal compression test reported here, can retard both swelling and deviatoric creep rates in the presence of significant swelling. However, the effect of compression compared to tension is asymmetric, producing a lesser response compared to tensile stresses of the same magnitude. Compressive uniaxial stresses greater than about 1.5 times the reference stress, σ_o, are required to reduce the total stress-free plus stress-affected swelling rate to zero.
e. The multiaxial creep and swelling data and the analyses of these data reported here provide support for use of the constitutive equations developed in Part I. These equations can be used by reactor core designers and analysts to predict irradiation damage-dependent distortion of complex structural components subject to gradients in neutron damage rate, temperature and stress state. Deviatoric creep and volumetric creep (stress-affected swelling) are each dependent on both deviatoric and hydrostatic components of stress.

7. Summary

The unique multiaxial creep-test specimens used in this study are shown capable of providing relatively well behaved in-reactor creep and swelling data. Constitutive equation parameters determined by analysis of the volumetric creep data, obtained from immersion density measurements, enable the prediction of the deviatoric creep data obtained independently from length and diameter data. The constitutive equations, which were developed in Part I according to the principles of incremental continuum plasticity, provide a faithful phenomenological representation of the data. These equations and the data analysis support an earlier observation that a deviatoric stress can affect volumetric swelling and show furthermore that deviatoric and volumetric creep are each dependent on both deviatoric and hydrostatic components of stress.

Acknowledgements

This experiment was conducted during the late 1970s under the auspices of the US Liquid Metal Reactor Program of the USDOE. The authors would like to thank Dr. F.A. Garner for making them aware of the relevance of this work to current reactor design needs and for his in-depth peer review and critique of the manuscript. M. Hall especially appreciates Dr. Garner's tutorial communications and his effort in providing references to the radiation damage literature.

References

[1] J.W. Bennett, J.H. Holmes, J.J. Laidler, US programs on reference and advanced cladding/duct materials, in: Conference on Radiation Effects in Breeder Reactor Structural Materials, 19 June 1977, Scottsdale, Arizona, USA, OSTI ID: 7289574.
[2] F.A. Garner, Irradiation performance of cladding and structural steels in liquid metal reactors, in: Nuclear Materials, Materials Science and Technology: A Comprehensive Treatment, vol. 10A, VCH Publishers, 1994, pp. 419–453 (Chapter 6).
[3] M.M. Hall, Jr., this issue.
[4] J.L. Straalsund, G.L. Guthrie, W.G. Wolfer, A diffusion model for the effect of applied stress on void and loop growth, in: Effects of Radiation on Substructure and Mechanical Properties of Metals and Alloys, ASTM STP 529, American Society for Testing and Materials, 1973, pp. 274–288.
[5] J.R. Matthews, M.W. Finnis, Journal of Nuclear Materials 159 (1988) 257–285.
[6] H.K. Sahu, P. Jung, Journal of Nuclear Materials 136 (1985) 154–158.
[7] T. Lauritzen, S. Vaidyanathan, W.L. Bell, W.J.S. Yang, Radiation-induced changes in microstructure, in: 13th International Symposium, Part I, STP 782, ASTM, Philadelphia, 1987. pp. 310–324.
[8] M.M. Hall Jr., Nuclear Technology 44 (1979) 172–176.
[9] A.S. Khan, S. Huang, Continuum Theory of Plasticity, J. Wiley and Sons, New York, 1995.
[10] E.E. Feldman, Nuclear Engineering and Design 53 (1979) 1–10.
[11] M.M. Hall Jr., Transactions of the American Nuclear Society 28 (1978) 146–147.
[12] J.R. Summers, A.G. Hins, M.M. Hall Jr., Transactions of the American Nuclear Society 28 (1978) 192.
[13] W.E. Ruther, S. Greenberg, Argonne National Laboratory, Report ANL-8042, 1973.
[14] J.E. Flinn, T.A. Kenfield, Swelling behavior of neutron irradiated stainless steel materials, in: Proceedings of the Workshop on Correlation of Neutron Damage and Charged Particle Damage, CONF-760673, US Dept. of Energy, Oak Ridge, TN, 1976, pp. 253–290.
[15] F.A. Garner, D.L. Porter, A reassessment of the swelling behavior of AISI 304L stainless steel, in: Proceedings of the International Conference on Dimensional Stability and Mechanical Behavior of Irradiated Metals and Alloys, vol. II, 11–13 April 1983, Brighton, England, pp. 41–44.
[16] F.A. Garner, Journal of Nuclear Materials 122 and 123 (1984) 459–471.
[17] T. Okita, N. Sekimura, T. Sato, F.A. Garner, L.R. Greenwood, Journal of Nuclear Materials 307–311 (2002) 322–326.
[18] F.A. Garner, B.J. Makenas, Recent experimental results on neutron-induced void swelling of AISI 304 stainless steel concerning its interactive dependence on temperature and displacement rate, in: Fontevraud-6 Symposium on Contribution of Materials Investigations to Improve the Safety and Performance of LWRs, 18–22 September 2006, Fontevraud, France, pp. 625–636.
[19] F.A. Garner, J.E. Flinn, M.M. Hall, B.J. Makenas, Recent insights on neutron-induced void swelling and irradiation creep of AISI 304 stainless steel, in: Proceedings of 13th International Conference on Environmental Degradation of Materials in Nuclear Power Systems, 19–23 August 2007, Whistler, Canada.
[20] J.E. Flinn, R.A. Weiner, G.L. Hoffman, Transactions of the American Nuclear Society 28 (1978) 224–225.
[21] G.L. Wire, J.L. Straalsund, Nuclear Technology 30 (1976) 71–76.
[22] T. Lauritzen, S. Vaidyanathan, W.L. Bell, W.J.S. Yang, Irradiation-swelling in AISI 316 steel: effect of tensile and compressive stresses, in: F.A. Garner, N.H. Packan, A.S. Kumar (Eds.), Radiation-Induced Changes in Microstructure: 13th International Symposium (Part I), ASTM STP 955, American Society for Testing and Materials, Philadelphia, 1987, pp. 101–113.
[23] S.J. Zinkle, G.E. Lucas, Deformation and fracture mechanisms in irradiated FCC and BCC metals, US Department of Energy, Fusion Materials 34, Semi-annual Report, June 2003, DOE-ER-0313/34, US DOE, Washington, DC, pp. 101–125.
[24] M.B. Toloczko, F.A. Garner, Journal of Nuclear Materials 212–215 (1994) 509–513.